remote sensing

MDPI

Article

DOA Estimation of Multiple Coherent Targets Using Weight Vector Orthogonal Decomposition in TDM-MIMO HF-Radar

Yifan Liu, Xin Zhang and Qiang Yang *

School of Electronics and Information Engineering, Harbin Institute of Technology, Harbin 150001, China; 22s005051@stu.hit.edu.cn (Y.L.); zhangxinhit@hit.edu.cn (X.Z.)
* Correspondence: yq@hit.edu.cn; Tel.: +86-136-1363-9936

Abstract: In recent years, MIMO high-frequency surface wave radar (MIMO-HFSWR) plays an increasingly important role in sea surveillance because of its wide-area surveillance capabilities. In signal processing, the coherent targets with the same distance and speed can only be distinguished in the angle dimension. However, HF radar's angular resolution is poor because of the restrictions of the aperture, which causes aliasing of targets on the range–angle (RA) spectrum. Traditional super-resolution algorithms, such as MUSIC, are also inapplicable because of the targets' coherence. Therefore, the spatial smoothing algorithm is usually used to realize the decoherence of echo at the cost of array aperture. The loss of array aperture makes the algorithm fail when there are too many targets in the echo. Aiming at this problem, this paper proposes an iterative calculation method (iterative calculation via weight vector orthogonal decomposition, IC-WORD) to estimate the angle of multiple coherent targets. Through the verification of simulation, it is proved that IC-WORD has better performance than the traditional spatial smoothing algorithm. More specifically, IC-WORD can correct spectral peak shift, improve angle measurement accuracy, and still operate stably under the condition of multiple coherent targets. This paper also uses the measured data from one of the most advanced HFSWR stations in China to validate the algorithm, which makes the paper have strong practical significance.

Keywords: MIMO-HFSWR; DOA estimation; multiple coherent sources; orthogonal decomposition

Citation: Liu, Y.; Zhang, X.; Yang, Q. DOA Estimation of Multiple Coherent Targets Using Weight Vector Orthogonal Decomposition in TDM-MIMO HF-Radar. *Remote Sens.* **2023**, *15*, 4073. https://doi.org/10.3390/rs15164073

Academic Editor: Yukiharu Hisaki

Received: 19 June 2023
Revised: 7 August 2023
Accepted: 14 August 2023
Published: 18 August 2023

1. Introduction

1.1. Development of MIMO HF-Radar

High-frequency surface wave radar (HFSWR), which operates in the 3–30 MHz frequency band, can detect targets over the horizon. However, the antenna array on HFSWR is quite massive, resulting in an overly large footprint and insufficient flexibility. multiple input multiple output (MIMO) technology was first applied to radar at the beginning of the 21st century. It can be combined with HFSWR by using the orthogonality of the transmit signals, allowing radar systems to achieve larger virtual array apertures with smaller array sizes. Time-division, frequency-division, and code-division multiplexing are the most common approaches for achieving transmit signal orthogonality. The time-division multiplexing MIMO (TDM-MIMO) radar system is the most commonly used because it is simple to operate and has a low design cost.

So far, multiple countries have conducted varying degrees of research in the field of MIMO-HFSWR. In 2014, Germany's WERA constructed a centralized MIMO-HFSWR experimental system [1,2], demonstrating the significant application value of MIMO-HFSWR. France conducted an experiment with an MIMO-HFSWR system in 2015 [3], demonstrating simultaneous receipt of four FMCW signals and a virtual aperture beam width of 1°. In 2017, Wuhan University of China tested a MIMO radar system of sky and earth waves, emitting signals of various frequencies and receiving echoes simultaneously across multiple channels, accomplishing the function of simultaneous sea-state detection of multiple frequencies [4].

MIMO technology for HFSWR is now mostly theoretical, with little research combined with actual systems. This paper uses the measured data collected by one of the most advanced HFSWR stations in China, which gives the paper strong practical significance.

1.2. Development of Multi-Coherent-Targets DOA Estimation

Conventional beam forming (CBF) [5], minimum variance distortionless response (MVDR), also known as Capon's method [6], multiple signal classification (MUSIC), estimation of signal parameters via rotational invariance techniques (ESPRIT) [7], and weighted subspace fitting (WSF) [8,9] are early mainstream DOA estimation algorithms. According to whether subspace decomposition is required, current decoherence methods can be divided into two classes: subspace decomposition algorithms and non-subspace decomposition algorithms, as illustrated in Figure 1:

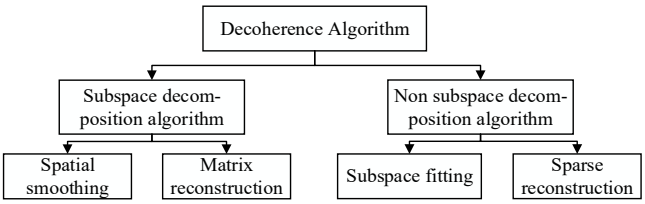

Figure 1. Classification of mainstream decoherence algorithms.

Subspace decomposition algorithm is generally based on MUSIC, ESPRIT improvement algorithm, and can be split into spatial smoothing algorithm and matrix reconstruction algorithm depending on the ways to decoherence. Although the above two types of algorithms have different ideas, the end result is signal decoherence at the cost of array aperture benefit. The representative algorithms have frequency or polarization or other transform domain smoothing algorithms [10–13], improved rotation subspace invariant method [14], Toeplitz approximation method [15–17], virtual array transformation method [18], and so on. Non-subspace decomposition decoherence algorithms primarily include subspace fitting algorithms and compressed sensing-theory-based sparse reconstruction algorithms. WSF, maximum likelihood (ML) method [19–21], and its improved algorithm are the primary subspace fitting algorithms. This type of algorithm has a higher utilization rate of array elements and better measurement performance, but it requires multidimensional nonlinear search and optimization, which need to be optimized using the alternating projection (AP) method [22], multi-level Wiener filtering method [23], or others during the iterative update procedure. The process mentioned above makes this type of algorithm have extremely high computational demand and it is difficult to apply in practice. Sparse reconstruction algorithms introduce compressed sensing (CS) into DOA estimation and generally need to construct an overcomplete basis matrix through grid processing. The grid mismatch problem [24] will occur if the DOA value of the real target is not on the grid points of the overcomplete base matrix, which will result in failure, and the orthogonal matching pursuit (OMP) algorithm [25] must be introduced to overcome the mismatch problem, which has an impact on the accuracy of such algorithms. In recent years, DOA estimation method is often combined with the related techniques of clutter suppression [26,27] and gradually developed into a composite technique.

In the DOA estimation process of the IC-WORD algorithm proposed in this paper, the orthogonal decomposition is needed to minimize the interaction between different signals and make the echoes in each direction tend to be independent to counter the influence of the coherence between targets on DOA estimation. The specific advantages will be shown in Section 4.

1.3. Origin of the IC-WORD Algorithm

In 2018, X. Zhang proposed an arbitrary array pattern synthesis method based on weight vector orthogonal decomposition (WORD algorithm) [28,29] that can design the

weight vector to make the array pattern meet specific requirements with low computational complexity and high degrees of freedom.

This paper proposes a spatial spectrum iterative calculation algorithm based on WORD (IC-WORD algorithm) that can be used in high-frequency TDM-MIMO radar for DOA estimation of coherent targets. To demonstrate its effectiveness, this paper compares DOA estimation using IC-WORD with DOA results obtained using algorithms such as spatially smoothed MUSIC (Smooth-MUSIC). It is shown that the algorithm developed in this paper can achieve higher angle measurement accuracy and the ability to detect more targets.

2. Signal Model

MIMO radar system uses arrays to transmit orthogonal signals, and the multiple signals are kept independent in space before being received. Compared to single-input multiple-output (SIMO) radar systems, MIMO radar systems can obtain signals with the same number of channels using fewer antennas. Using the MIMO radar with two transmitting antennas and four receiving antennas (T2R4) as an example, the arrays are arranged on the same line and the distance between transmitting antennas is four times that of receiving antennas, as shown in the following figure.

As shown in Figures 2 and 3, MIMO radar achieves the same performance as SIMO radar with fewer array elements and smaller array size. However, MIMO radar requires the transmit signal to be orthogonal, which can be accomplished in three ways: time-division multiplexing, frequency-division multiplexing, and code-division multiplexing. In this paper, time-division multiplexing is used because it does not require waveform modulation or encoding and only requires signal orthogonality in the time dimension, which can be achieved through transmitting the same signal waveform in different time.

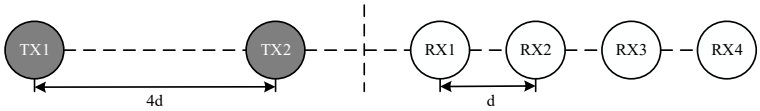

Figure 2. T2R4-MIMO radar layout diagram.

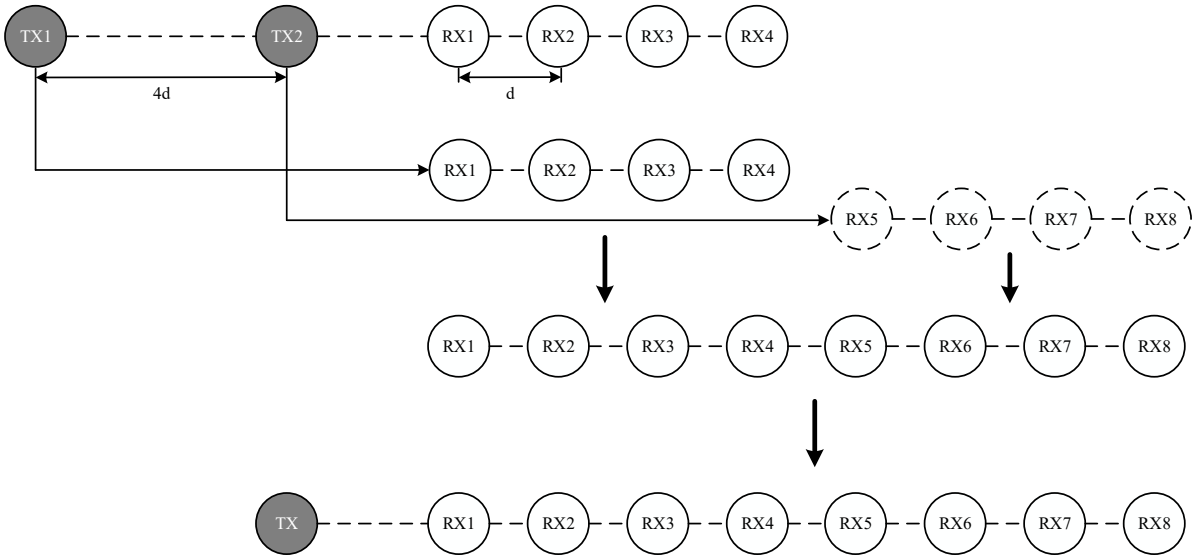

Figure 3. T2R4-MIMO equivalent virtual array: T1R8-SIMO.

In Figures 2 and 3, TX is the transmitting array and RX is the receiving array and the T2R4-MIMO array can be equated to the following T1R8-SIMO array. ”d” represents the distance between receiving antennas. And the distance between transmitting antennas is four times that of receiving antennas.

Assuming the radar transmits a linear frequency modulation (LFM) signal, the TDM-MIMO transmit signal of T2R4 is schematically depicted in the figure below.

In Figure 4, black line represents the signal transmitted by TR1, red represents TR2, Ts represents the FM period, and the structure of the T2R4-TDM-MIMO radar system can be represented by Figure 5.

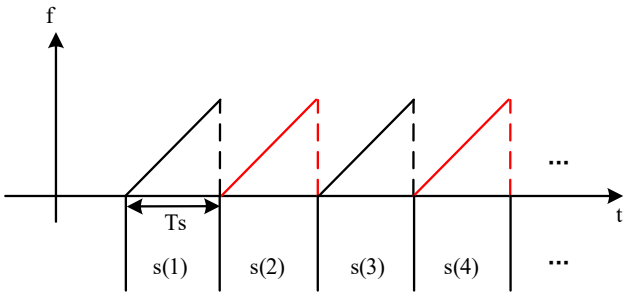

Figure 4. TDM-MIMO transmit signal.

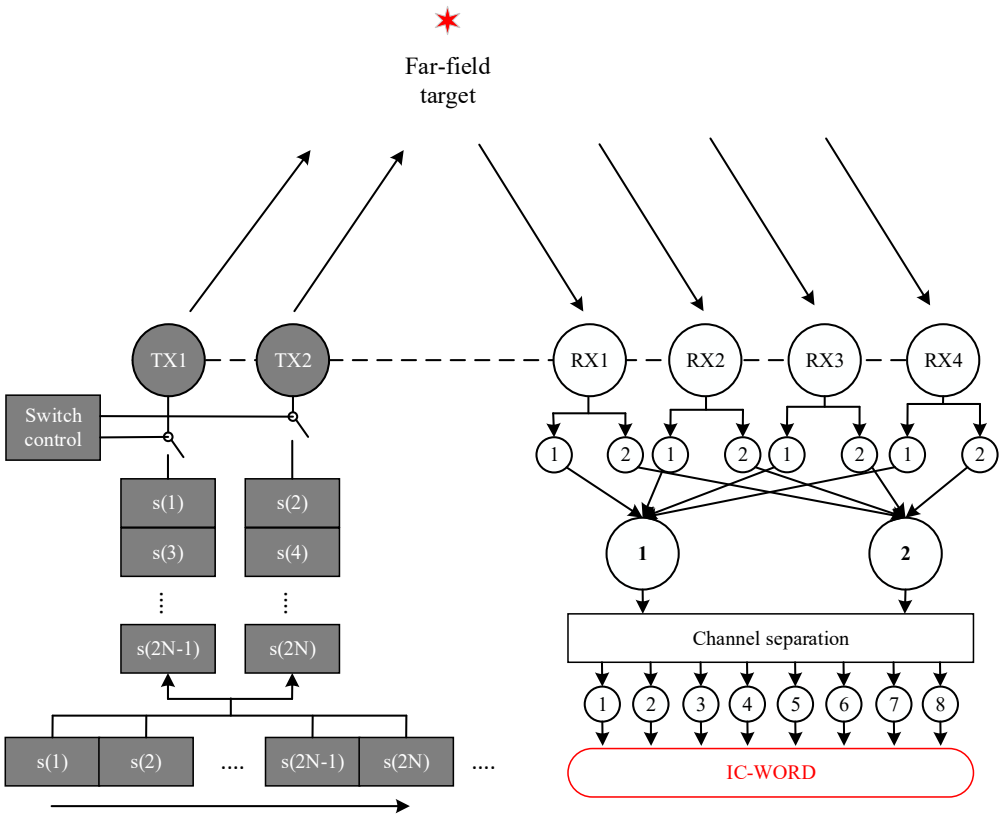

Figure 5. The structure of T2R4-TDM-MIMO radar system.

As shown in Figure 5, T2R4-MIMO radar can obtain eight independent channels after channel separation. Then, the signal from all channels will be entered into the IC-WORD algorithm for subsequent processing. The brief process of the IC-WORD algorithm is shown in the Figure 6.

As shown in the figure above, the IC-WORD algorithm carries out multiple weighted summations of the eight-channel signals (from ① to ⑧) to obtain the spatial spectrum, which is the first iteration process discussed in Section 3.2.1.

Using the spatial spectrum obtained in the first iteration, the weights are redesigned by WORD algorithm (Section 3.1) and the spatial spectrum is recalculated with new weights, which is the process of the second iteration (Section 3.2.2). The third iteration uses the spatial spectrum obtained in the second iteration to redesign the weights and calculate a

new spatial spectrum, and so on. After each iteration, it is necessary to determine whether to terminate the algorithm according to Section 3.2.3.

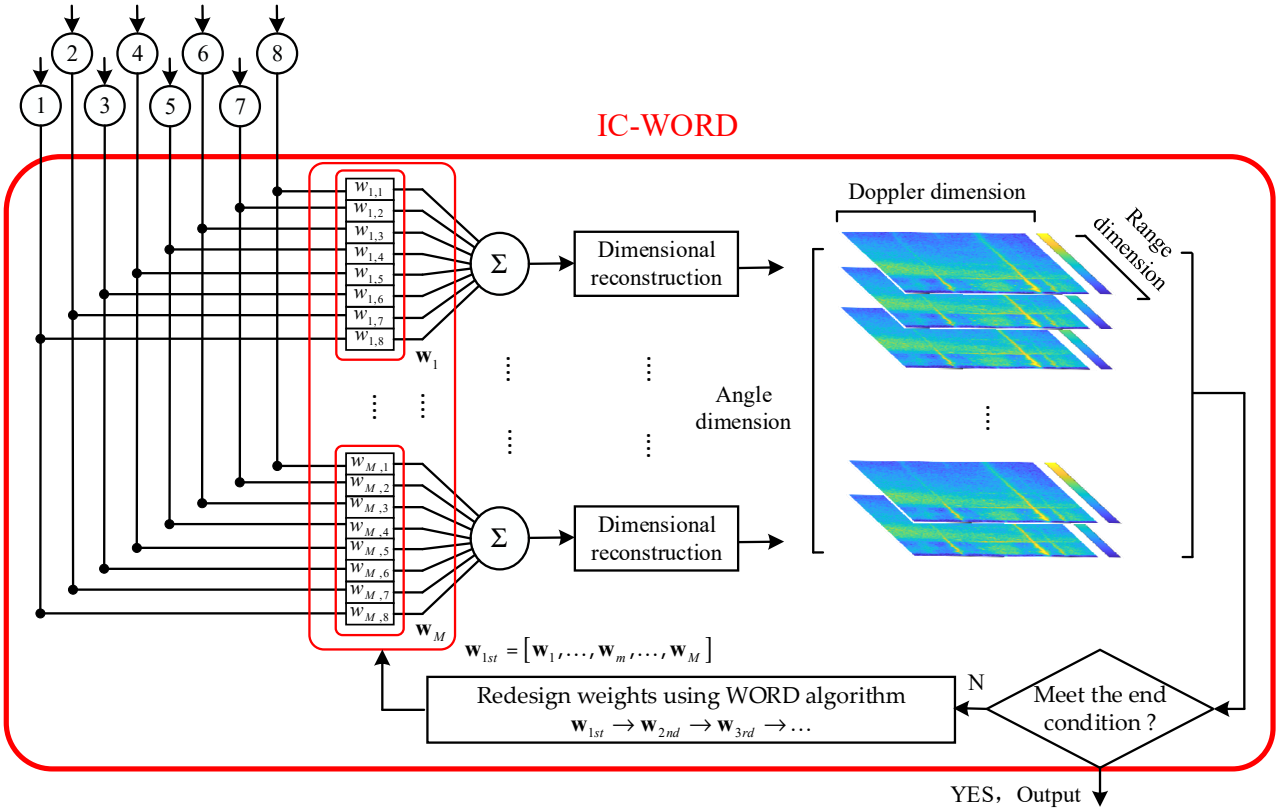

Figure 6. The brief process of IC-WORD algorithm.

The above is only a brief description of the IC-WORD algorithm. Section 3 will provide a detailed introduction to the algorithm.

When considering the more general TDM-MIMO radar system of N1 transmitting arrays and N2 receiving arrays, there will be a total of N1 times N2 channels of signal, where the signal transmitted by the n1-th antenna and received by the n2-th antenna can be expressed as:

$$s_{n_1 n_2}(t) = A \cdot rect\left(\frac{t - t_r}{\tau}\right) \exp\left(j2\pi\left((f_0 - f_d)(t - t_r) + \frac{1}{2}\mu(t - t_r)^2\right) + \phi_{n_1 n_2}\right) \quad (1)$$

where $rect(t/\tau)$ represents a square pulse signal of length τ, f_0 represents the center frequency of the transmit signal, μ represents the FM slope, t_r represents the time difference between transmitting and receiving signals, f_d represents the Doppler shift due to the target movement, and $\phi_{n_1 n_2}$ represents the relative phase shift of the received signal.

Assuming that the targets are stationary, the echo in this case can be expressed as:

$$s_{n_1 n_2}(t) = A \cdot rect\left(\frac{t - t_r}{\tau}\right) \exp\left(j2\pi\left(f_0(t - t_r) + \frac{1}{2}\mu(t - t_r)^2\right) + \phi_{n_1 n_2}\right) \quad (2)$$

At this point, the total number of channels is $N_1 \times N_2$ and we can calculate the phase difference from the relative phase matrix $\Phi = [\phi_1, \ldots, \phi_{n_1 n_2}, \ldots, \phi_{N_1 N_2}]$ of multiple channels to obtain the angle of the target relative to the receiving array.

3. Theory and Analysis

3.1. Pattern Synthesis via Weight Vector Orthogonal Decomposition (WORD Algorithm)

Consider an arbitrary structured array with a total number of virtual elements of N. When the signal direction of a far-field target is θ, the array steering vector of this signal can be expressed as:

$$\mathbf{a}(\theta) = \left[g_1(\theta)e^{-j\omega\tau_1(\theta)}, \ldots, g_N(\theta)e^{-j\omega\tau_N(\theta)}\right]^T \tag{3}$$

where $g_n(\theta)$ represents the amplitude change caused by the antenna itself and $\tau_n(\theta)$ represents the phase difference of signal from different channels. Now, use a weight vector $\mathbf{w} = [w_1, \ldots, w_N]^T$ to weight this array and the beam pattern of this array after weighting can be expressed as:

$$P(\theta) = \sum_{n=1}^{N} {w_n}^* g_n(\theta)e^{-j\omega\tau_n(\theta)} = \mathbf{w}^H\mathbf{a}(\theta) \tag{4}$$

where $(\cdot)^*$ and $(\cdot)^H$ denote the transposition and conjugate transposition operations and $P(\theta)$ is the array response at θ ($\theta \in [-\pi, \pi]$), whose power is defined as:

$$|P(\theta)|^2 = \left|\sum_{n=1}^{N} {w_n}^* g_n(\theta)e^{-j\omega\tau_n(\theta)}\right|^2 = \left|\mathbf{w}^{\mathrm{H}}\mathbf{a}(\theta)\right|^2 \tag{5}$$

Assuming that the desired array pattern is $P_d(\theta)$, the general beamforming problem can be described as finding a suitable weight vector $\mathbf{w}$ such that the array pattern $P(\theta)$ satisfies the desired pattern $P_d(\theta)$. The general idea of $P_d(\theta)$ is to maximize the array response in every look direction (θ) and minimize the responses from sidelobe directions, so that, if a target is present in the look direction, its response will not be affected by those of other targets present in other directions. Subsequent iterations include array-response information from all targets, as will be shown in the development in this paper. The above problem can be expressed using Formula (6):

$$\begin{array}{ll} find & \mathbf{w} \in C^N \\ s.t. & P(\theta) \approx P_d(\theta), \theta \in [-90^{\mathrm{o}}, 90^{\mathrm{o}}] \end{array} \tag{6}$$

As shown above, the main problem of beamforming is to find or design a suitable weight $\mathbf{w}$ so that the array pattern $P(\theta)$ can be consistent with the desired pattern $P_d(\theta)$, and WORD algorithm is precisely used to solve this problem.

The WORD algorithm realizes the overall shape design of the pattern through multiple single-point adjustments of the pattern [28]. It will first obtain the desired main lobe direction and generate the initial weight according to it and then adjust the weight's beam pattern point by point according to the desired pattern. Finally, a weight vector is obtained whose beam pattern perfectly matches the desired pattern. In summary, the function of the WORD algorithm is to obtain a weight vector that satisfies the desired pattern. The whole process of WORD algorithm is shown in the Figure 7.

As shown in Figure 7, by adjusting each point (the red circle in the beam pattern indicates the position of the point to be adjusted), WORD can obtain the weight whose beam pattern consistent with the desired pattern.

The mathematical process of WORD is to decompose the weight vector into two orthogonal vectors: one of them is parallel to the array steering vector $\mathbf{a}(\theta_{k+1})$ corresponding to the angle θ_{k+1} that needs to be controlled at the $k+1$ step of the iteration, while the other vector is orthogonal to $\mathbf{a}(\theta_{k+1})$, as shown in the following figure.

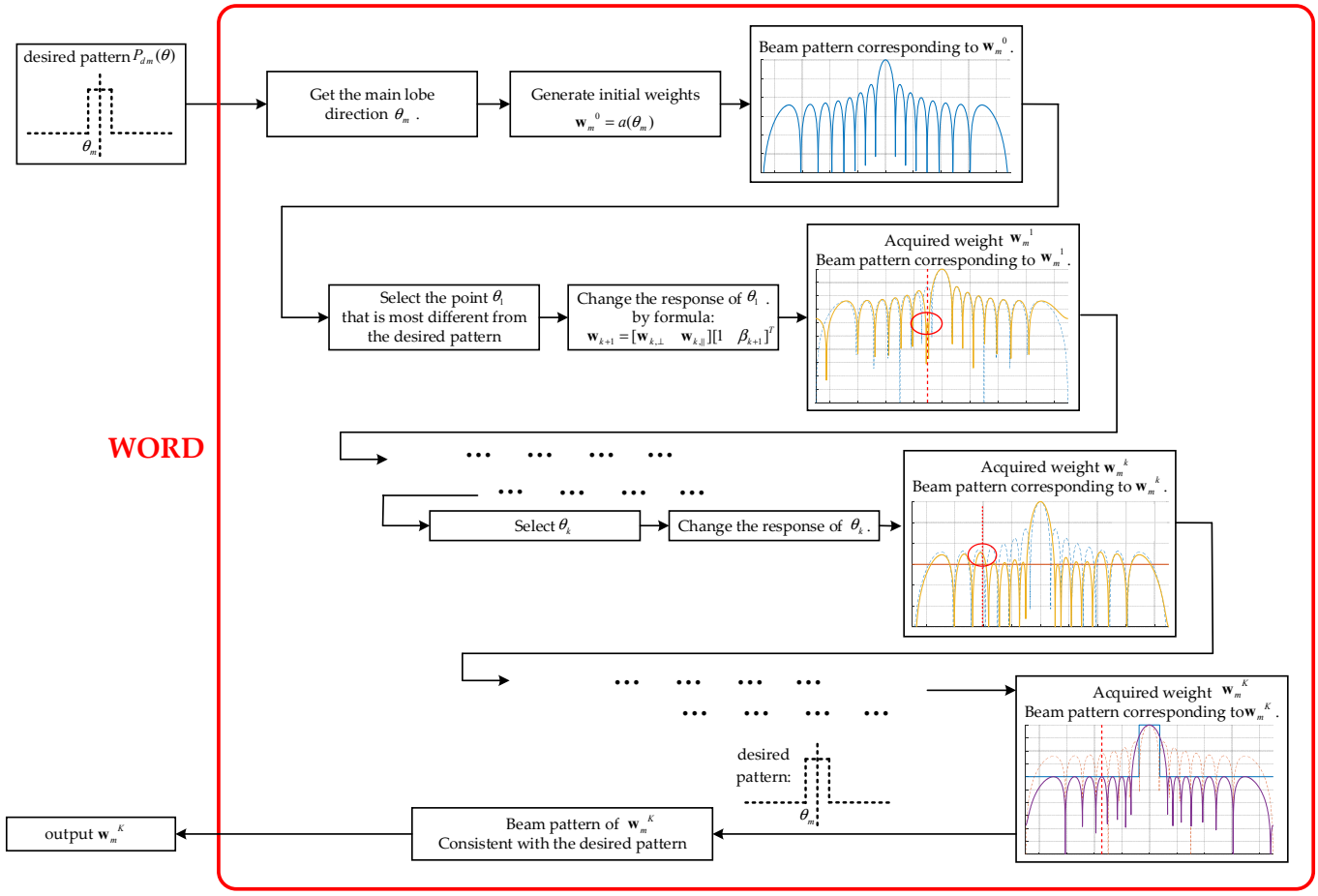

Figure 7. The process of WORD algorithm.

As shown in Figure 8, when weight vector iteration of step k results in $\mathbf{w}_k$, weight $\mathbf{w}_{k+1}$ of step $k+1$ can be represented by two orthogonal vectors ($\mathbf{w}_{k,\perp}$ and $\mathbf{w}_{k,\|}$):

$$\mathbf{w}_{k+1} = [\mathbf{w}_{k,\perp} \quad \mathbf{w}_{k,\|}][1 \quad \beta_{k+1}]^T \tag{7}$$

where β_{k+1} is a coefficient to be found and the expressions of the other two orthogonal vectors are:

$$\begin{aligned} \mathbf{w}_{k,\perp} &= \mathbf{P}^{\perp}_{[\mathbf{a}(\theta_{k+1})]}\mathbf{w}_k \\ \mathbf{w}_{k,\|} &= \mathbf{P}_{[\mathbf{a}(\theta_{k+1})]}\mathbf{w}_k \end{aligned} \tag{8}$$

where $\mathbf{P}_{[\mathbf{a}(\theta_{k+1})]}$ and $\mathbf{P}^{\perp}_{[\mathbf{a}(\theta_{k+1})]}$ are the orthogonal projection matrix and the orthogonal projection complement matrix determined by $\mathbf{a}(\theta_{k+1})$, which is also the orthogonal projection matrix to the column space of $\mathbf{a}(\theta_{k+1})$ and the orthogonal subspace of its column space, respectively, expressed in the following form:

$$\begin{aligned} \mathbf{P}_{[\mathbf{a}(\theta_{k+1})]} &= \frac{\mathbf{a}(\theta_{k+1})\mathbf{a}^{\mathrm{H}}(\theta_{k+1})}{\mathbf{a}(\theta_{k+1})_2^2} \\ \mathbf{P}^{\perp}_{[\mathbf{a}(\theta_{k+1})]} &= \mathbf{I} - \mathbf{P}_{[\mathbf{a}(\theta_{k+1})]} \end{aligned} \tag{9}$$

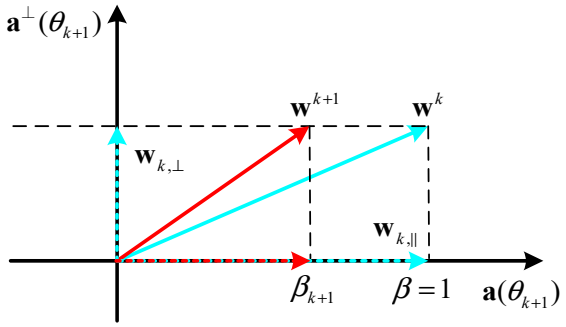

Figure 8. Orthogonal decomposition of weight vector.

The WORD algorithm gives two solutions for β_{k+1} as:

$$\begin{aligned}\beta_{k+1,a} &= \frac{-\mathrm{Re}(\mathbf{B}(1,2))+d}{\mathbf{B}(2,2)}\\ \beta_{k+1,b} &= \frac{-\mathrm{Re}(\mathbf{B}(1,2))-d}{\mathbf{B}(2,2)}\end{aligned} \tag{10}$$

where $\mathrm{Re}(\cdot)$ denotes the real part of complex numbers, and the construction expression of matrix B is:

$$\mathbf{B} = \begin{bmatrix} -\rho_{k+1}\left|\mathbf{w}_{k,\perp}^{\mathrm{H}}\mathbf{a}(\theta_0)\right|^2 & -\rho_{k+1}\mathbf{w}_{k,\perp}^{\mathrm{H}}\mathbf{a}(\theta_0)\mathbf{a}^{\mathrm{H}}(\theta_0)\mathbf{w}_{k,\parallel} \\ -\rho_{k+1}\mathbf{w}_{k,\parallel}^{\mathrm{H}}\mathbf{a}(\theta_0)\mathbf{a}^{\mathrm{H}}(\theta_0)\mathbf{w}_{k,\perp} & \left|\mathbf{w}_{k,\parallel}^{\mathrm{H}}\mathbf{a}(\theta_{k+1})\right|^2 - \rho_{k+1}\left|\mathbf{w}_{k,\parallel}^{\mathrm{H}}\mathbf{a}(\theta_0)\right|^2 \end{bmatrix} \tag{11}$$

where $\rho_{k+1} = |P(\theta_{k+1})|^2/|P(\theta_0)|^2 = \left|\mathbf{w}_{k+1}^{\mathrm{H}}\mathbf{a}(\theta_{k+1})\right|^2/\left|\mathbf{w}_{k+1}^{\mathrm{H}}\mathbf{a}(\theta_0)\right|^2$, which represents the level corresponding to the angle that needs to be adjusted in step $k+1$.

The expression of the constant d is:

$$d = \sqrt{[\mathrm{Re}(\mathbf{B}(1,2))]^2 - \mathbf{B}(1,1)\mathbf{B}(2,2)} \tag{12}$$

After that, the coefficient that minimizes the difference between the pattern of the current step and the previous step among the two solutions of β_{k+1} is selected as the final coefficient, i.e., the β_{k+1} with the smallest $F(\beta)$ is selected as the final result, and the expression of $F(\beta)$ is as follows:

$$F(\beta) = \left\| \mathbf{P}^{\perp}_{[\mathbf{w}_{(k)}]} \frac{\mathbf{w}_{k+1}}{\|\mathbf{w}_{k+1}\|_2} \right\|_2 \tag{13}$$

The above is the mathematical process of array-response adjustment by WORD. After each iteration of this adjustment process, the array response in every angular look direction $P(\theta_{k+1})$ of $P(\theta)$ can become closer to that of the desired response $P_d(\theta_{k+1})$. The response adjustment at each look-direction point in θ can make $P(\theta)$ as a whole meet the requirements of $P_d(\theta)$ by iterating. Regarding the selection of the angle θ_k for adjustment, the principle can be expressed as follows:

$$\theta_k = \underset{\theta\in\Omega}{\mathrm{argmax}}(|P_d(\theta) - P_{k-1}(\theta)|) \tag{14}$$

where θ_k is the angle to be adjusted in the k step, $P_d(\theta)$ is the desired pattern, $P_{k-1}(\theta)$ is the temporary pattern obtained after the last $k-1$ step, and Ω is the set of adjustable angles. In brief, the angle points in $P_{k-1}(\theta)$ with the largest difference from $P_d(\theta)$ are selected for adjustment in step k.

After the above adjustment, the desired weight vector **w** is obtained whose array response $P(\theta)$ can substantially match the desired pattern $P_d(\theta)$.

3.2. Spatial Spectrum Iterative Calculation Method Based on Weight Vector Orthogonal Decomposition (IC-WORD)

Using the WORD algorithm, we can obtain the weights **w** corresponding to the desired pattern $P_d(\theta)$. This optimization using WORD is meant to shape the array pattern of the scan vector $\mathbf{a}(\theta)$ as θ is scanned across the field of view by applying weights to its elements so as to minimize responses from sidelobes and maximize response in the look direction at each value of theta in the field of view.

The IC-WORD method requires multiple designs of the weight vector **w** and multiple rounds of iteration to obtain the spatial spectrum in order to achieve the highest goniometric accuracy. WORD algorithm is a tool used by IC-WORD algorithm to design weights according to the desired pattern. The core of the WORD algorithm is how to obtain weights based on requirements, while the core of the IC-WORD algorithm is how to propose requirements to achieve better spatial spectral result. The desired pattern requirements are obtained from the previous iteration of array weights, which are used to obtain an array response pattern at every look direction in the presence of all target echoes. Thus, the array response of the next iteration can be further optimized to have a maximum for the current look direction and minimal responses from other directions, including those of targets not at the look direction.

3.2.1. The First Iteration

Before the iteration begins, the angle region that needs to be calculated from -90 degree to 90 degree is divided evenly into M regions. For example, $[-90^\circ, 90^\circ]$ is divided evenly into 180 regions at 1-degree intervals, which means M = 180. Then, each iteration requires the design of 180 weight vectors, each of which is applied to calculate the echo power of its corresponding angle region. These 180 points make up the entire spatial spectrum.

In practical applications, it is usually not necessary to divide the angle region at 1-degree intervals, often at intervals of 3 degrees. This can accelerate the calculation speed, as each iteration only needs to design 60 weight vectors. In order to maximize the details of the spatial spectrum, this article divides 180 regions at one-degree intervals. The schematic diagram is shown in Figure 9.

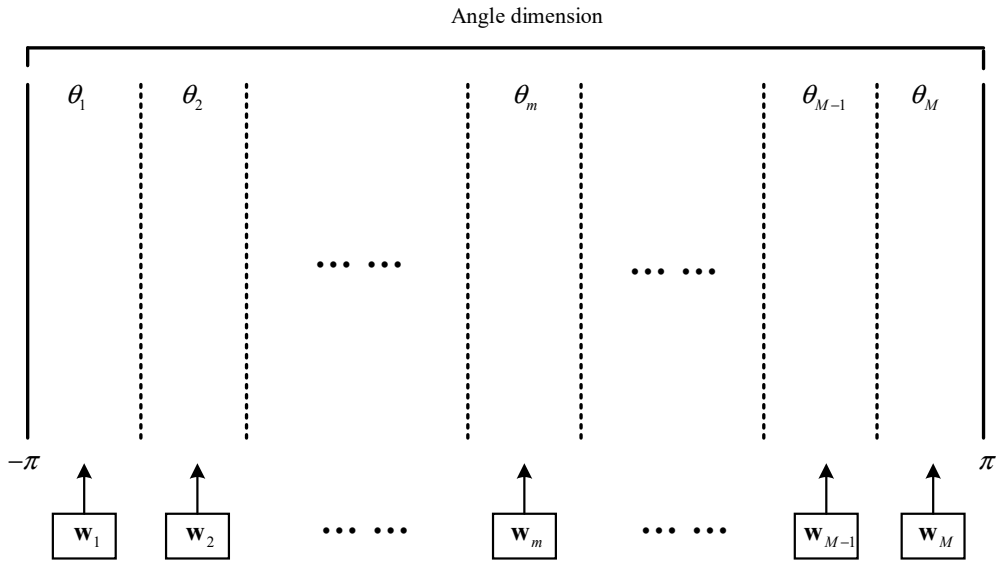

Figure 9. Angle region division.

As shown above, when calculating the received power in the $m-$ th region, we need to design the weights as $\mathbf{w}_m$ to minimize the impact of other directions and there are a total of M weights. The weight matrix of the first iteration is defined as:

$$\mathbf{w}_{1st} = [\mathbf{w}_1, \ldots, \mathbf{w}_m, \ldots, \mathbf{w}_M] \tag{15}$$

The matrix of the set of desired patterns is defined as:

$$P_{d-1st}(\theta) = [P_{d1}(\theta), \ldots, P_{dm}(\theta), \ldots, P_{dM}(\theta)] \tag{16}$$

Design guidelines for $P_{d-1st}(\theta)$: taking the $m-$ th angular region as an example, $\mathbf{w}_m$ of $\mathbf{w}_{1st}$ is used for calculating the power of the echo in that direction, and its corresponding array response is $P_m(\theta)$. In order to avoid the influence of other regions, the desired pattern $P_{dm}(\theta)$ is in the form of the main lobe pointing to the angular center θ_m of the $m-$ th region and the sidelobe suppressed to $A_{sidelobe}$; since no information about the echo is obtained at this time, the sidelobe level here cannot be designed to a complex shape, and a certain value should be chosen according to the specific situation, for example, -30 dB. The lower the sidelobe level we desired, the wider the main lobe will be and the longer the time the algorithm will use. The mathematical representation of the above process is as follows:

$$\begin{array}{ll} find & \mathbf{w}_m \in C^N \\ s.t. & P_m(\theta) \approx P_{dm}(\theta) \\ s.t. & P_{dm}(\theta_m) = 0 \\ s.t. & P_{dm}(\theta_{el}) = A_{sidelobe} \end{array} \tag{17}$$

where $P_m(\theta)$ is the array pattern corresponding to $\mathbf{w}_m$, $P_{dm}(\theta)$ is the desired pattern of the m region, θ_m is the angular center position of this region, θ_{el} is the angular range except for the main lobe pointing to θ_m, and the weight $\mathbf{w}_m$ corresponding to the m region can be obtained from the above calculation process. The first iteration's final result is $\mathbf{w}_{1st} = [\mathbf{w}_1, \ldots, \mathbf{w}_m, \ldots, \mathbf{w}_M]$.

Assuming that the received signal of the MIMO radar is S_r, its spatial spectrum SP_{1st} can be expressed as:

$$\mathrm{SP}_{1st} = {\mathbf{w}_{1st}}^H S_r = \begin{bmatrix} {\mathbf{w}_1}^H \\ \vdots \\ {\mathbf{w}_M}^H \end{bmatrix} S_r = \begin{bmatrix} \mathrm{SP}_{1st}(\theta_1) \\ \vdots \\ \mathrm{SP}_{1st}(\theta_M) \end{bmatrix} \tag{18}$$

where $\mathrm{SP}_{1st}(\theta_1)$ is the power of the first region, $\mathrm{SP}_{1st}(\theta_M)$ is the power of the M regions, and SP_{1st} is the spatial spectrum calculated in the first iteration. Note that ${\mathbf{w}_m}^H S_r$ represents a one-time weighted summation of multiple signals, whose power needs to be calculated to obtain $\mathrm{SP}_{1st}(\theta_m)$.

The process of the first iteration can be summarized as the process shown in Figure 10.

As shown above, in the first iteration process, the main lobes of the patterns of M weights point towards the center of their own angle regions. That is to say, in the first iteration of this article, the main lobes of w1 point towards 89.5°, w2 point towards 88.5°, and so on. Due to the lack of prior information, the sidelobes of the weights' patterns do not require complex design. In Section 4, they are uniformly lowered to -30 dB. If a radar is used with a larger array aperture than that of this article, the sidelobes can be pressed lower.

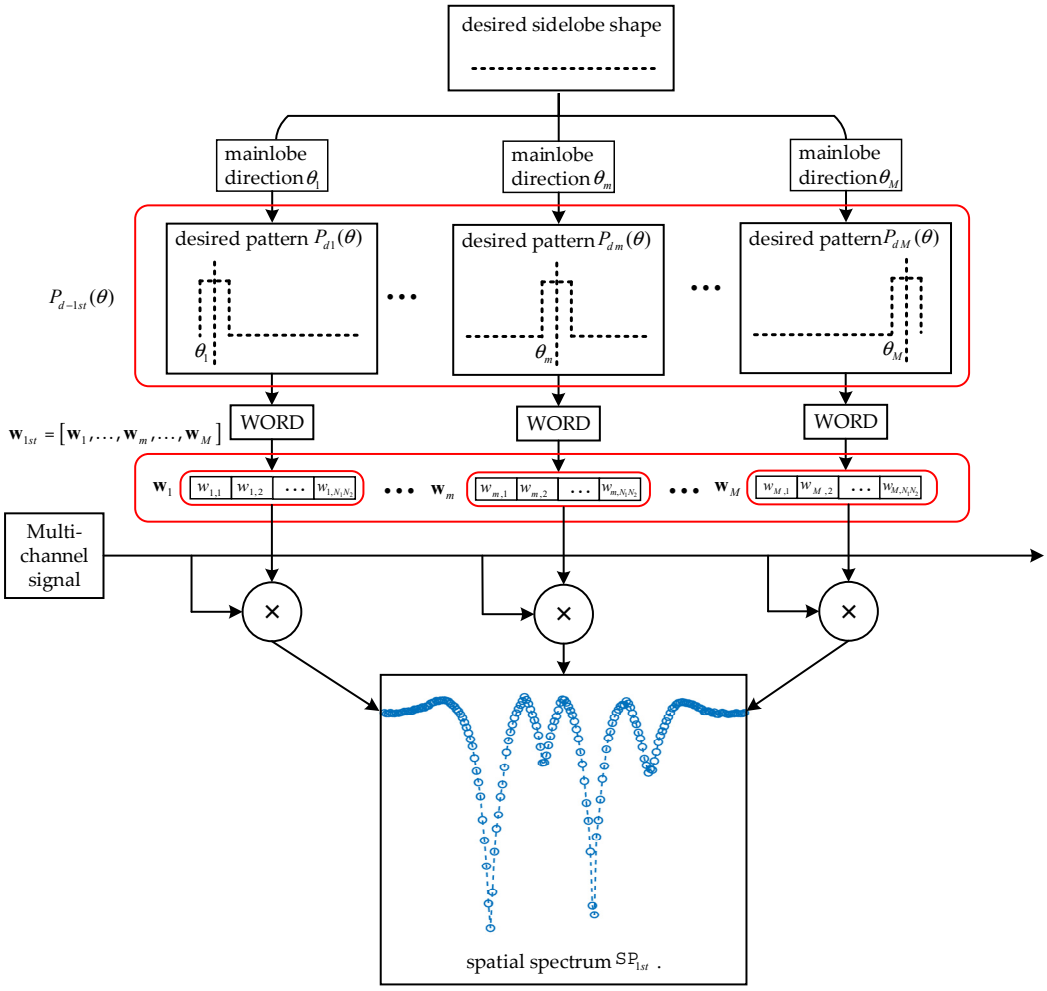

Figure 10. The first iteration of IC-WORD.

3.2.2. The Second Iteration

The second iteration's spectrum needs to be calculated on the basis of the first iteration, defining the second iteration weight matrix as:

$$\mathbf{w}_{2nd} = \left[\mathbf{w}_{1_2}, \ldots, \mathbf{w}_{m_2}, \ldots, \mathbf{w}_{M_2}\right] \tag{19}$$

The matrix of desired pattern composition for the second iteration is defined as:

$$P_{d-2nd}(\theta) = \left[P_{d1_2}(\theta), \ldots, P_{dm_2}(\theta), \ldots, P_{dM_2}(\theta)\right] \tag{20}$$

Design guidelines for $P_{d-2nd}(\theta)$: after obtaining the spatial spectrum SP_{1st} calculated in the first iteration, the inversion of SP_{1st} is taken and compressed to RA range (RA reference range is displayed in Table 1) as the sidelobe level guideline of the second iteration weight. The process is shown in the figure below.

Table 1. RA reference range.

Antenna Array	8 Elements	12 Elements	16 Elements
RA (dB)	[−37, −6.4]	[−41.5, −6.5]	[−46, −8]

As shown in Figure 11, after obtaining the spatial spectrum in the first iteration, the reciprocal of this spatial power spectrum is taken and compressed to the range RA. The result will serve as the sidelobe benchmark for the next iteration's weights. Based on this

benchmark, the next iteration will redesign the M sets of weights to obtain a new spatial spectrum.

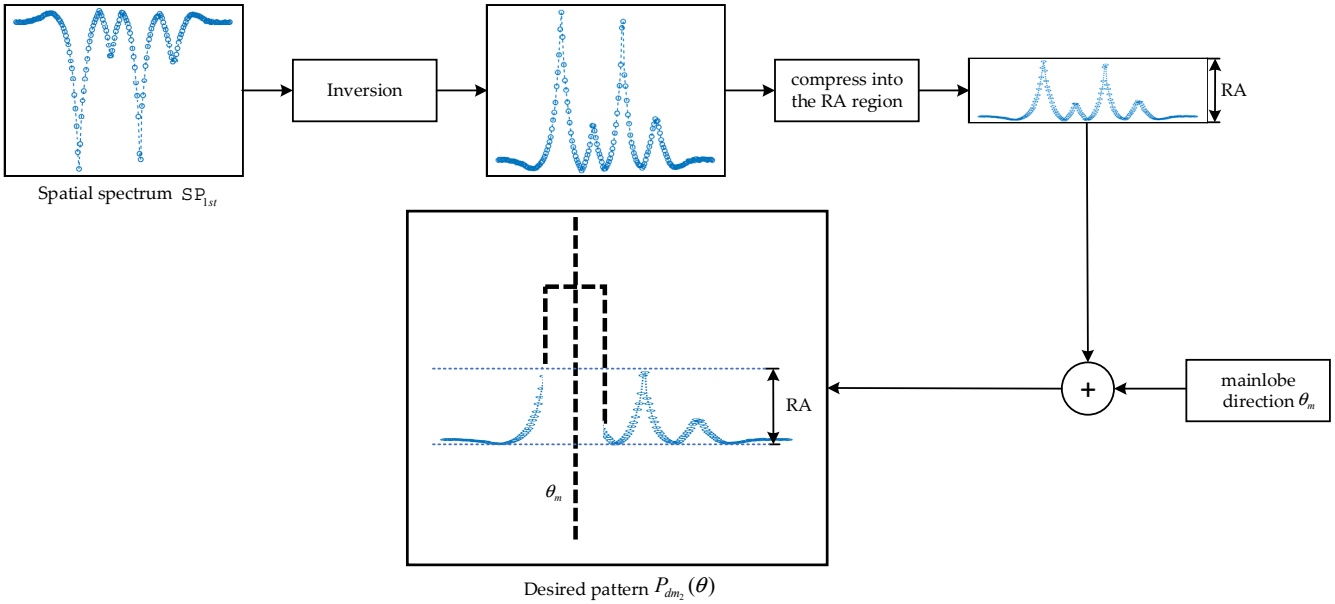

Figure 11. The process of designing the sidelobe of the second iteration according to the spatial spectrum of the first iteration.

RA may vary depending on the size of the array. In the process of weight design, insufficient suppression of sidelobes can result in less improvement; excessive pressure on the sidelobes can cause the main lobe to widen, leading to a significant decrease in angular resolution. To ensure the good performance of the IC-WORD algorithm, the upper limit of RA should be consistent with the first sidelobe level of digital beamforming under the same array condition and the lower limit should be at least three times the minimum sidelobe peak of digital beamforming. According to the test, some reference values for RA are given below.

This design can greatly reduce the impact of targets located at other directions when calculating the echo power in the current angle region, i.e., the look direction of the receiving array. The spatial spectrum of the second iteration will be better than that of the first.

The weight matrix $\mathbf{w}_{2nd}$ of the second iteration is defined as:

$$\mathbf{w}_{2nd} = \left[\mathbf{w}_{1_2}, \ldots, \mathbf{w}_{m_2}, \ldots, \mathbf{w}_{M_2}\right] \tag{21}$$

In addition, the weight design process of the second iteration can be expressed as:

$$\begin{array}{ll} find & \mathbf{w}_{m_2} \in C^N \\ s.t. & P_{m_2}(\theta) \approx P_{dm_2}(\theta) \\ s.t. & P_{dm_2}(\theta_m) = 0 \\ s.t. & P_{dm_2}(\theta_{el}) = R(\mathrm{SP}_{1st}(\theta_{el})) \end{array} \tag{22}$$

where $\mathbf{w}_{m_2}$ is the weight corresponding to the $m-$th angular region in the second iteration, $R(\cdot)$ represents inversion and compression, and $R(\mathrm{SP}_{1st}(\theta_{el}))$ is the desired sidelobe level.

The second iteration process is almost the same as the first, and the second iteration weight matrix $\mathbf{w}_{m_2}$ also contains M weights, which can be used to recalculate the spatial spectrum:

$$\mathrm{SP}_{2nd} = \mathbf{w}_{2nd}{}^{H} S_r = \begin{bmatrix} \mathbf{w}_{1_2}{}^{H} \\ \vdots \\ \mathbf{w}_{M_2}{}^{H} \end{bmatrix} S_r = \begin{bmatrix} \mathrm{SP}_{2nd}(\theta_1) \\ \vdots \\ \mathrm{SP}_{2nd}(\theta_M) \end{bmatrix} \tag{23}$$

The result SP_{2nd} of the second iteration will have higher angular resolution and angle measurement accuracy than SP_{1st}, which is verified in Section 4.1.

The process of the first iteration and the second can be summarized as the process shown in the Figure 12.

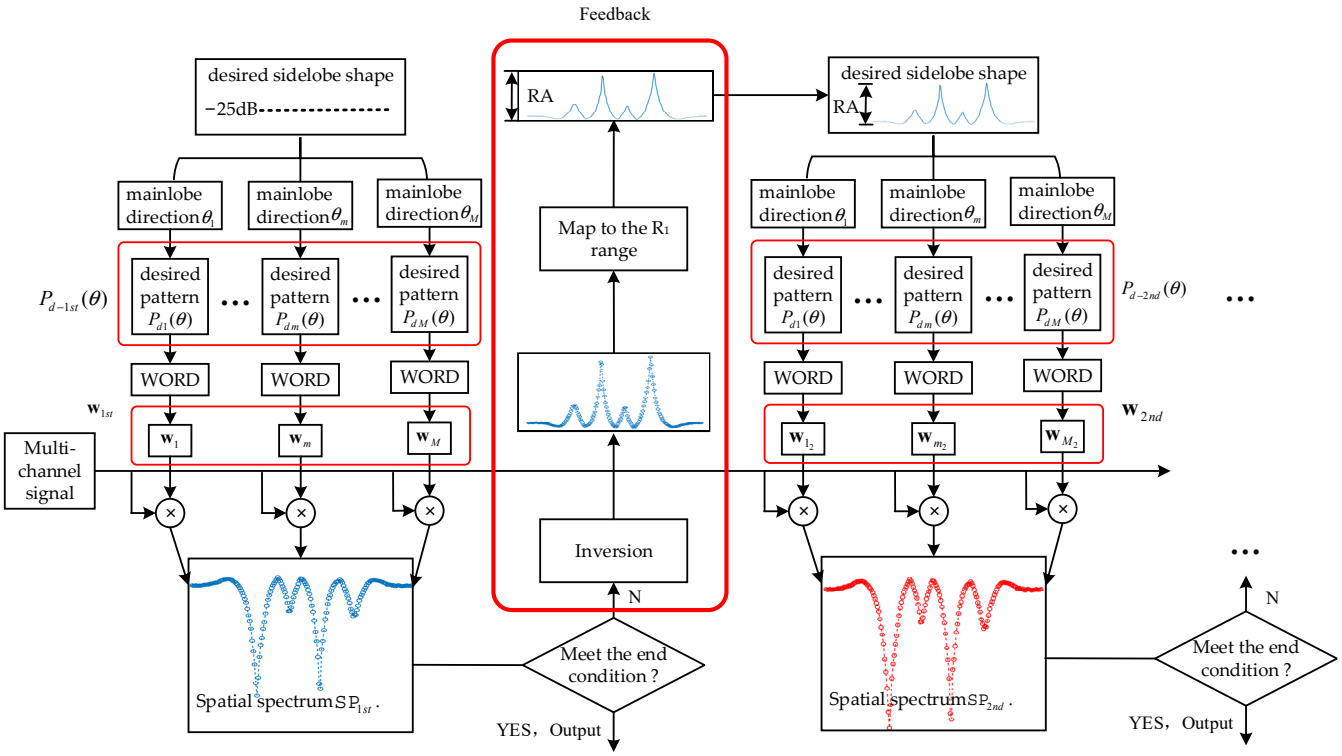

Figure 12. The first and the second iteration of IC-WORD.

As shown above, in the second iteration, the main lobes of the weights' pattern still point towards the center of their angle regions, but the sidelobes require a special design. The reciprocal of the spatial spectrum obtained in the first iteration is taken and compressed into the RA region.

According to the process of two iterations above, more iterations can be repeated to obtain a higher performance. In subsequent iterations of the scan-vector weights, the "desired" array response is the spatial spectrum's inversion, obtained by scanning and processing the target echoes in the field of view using the weights obtained for the scan vector in the previous iteration. It now contains information from all the targets, so its weights can be optimized to minimize their effect on targets not at the current look direction, when computing the spatial spectrum in the next iteration.

3.2.3. Algorithm Termination Condition

However, due to the aperture limitation of the physical array, the angle resolution and accuracy cannot be improved infinitely, and too many iterations will only increase computational complexity but not obtain significant improvement.

Therefore, two thresholds are defined as the divergence threshold THd and the convergence threshold TH to terminate the algorithm at a suitable moment.

When the difference between the weights of the two iterations is less than the convergence threshold TH, it can be considered that the performance improvement brought by

iteration is too small to continue calculating and the current iteration will be the end of the algorithm.

The divergence threshold THd is a protection of the algorithm, which is defined as the difference of the weights between the first iteration and the second. Because the difference between the weights of the first and second round of the iteration is often the largest, the adjustment in subsequent iterations is relatively small. When the subsequent difference between weights is larger than the difference between the first two rounds, it can be considered that there is a problem during the weight design process. For example, the divergence threshold THd of the first angle region can be expressed as:

$$THd = \left\| \mathbf{w}_{1_2} - \mathbf{w}_1 \right\| \tag{24}$$

The following explains why these two thresholds are required as termination conditions: as the iteration proceeds, the angle resolution and accuracy of the spatial spectrum will gradually improve; at this time, the depression between the two targets will become lower and sharper. When the sharpness of the depression reaches a certain level, the requirements will be too strict for physical arrays, which will lead to the failure of the weights to reach the desired pattern within a limited number of adjustments. In this case, the spatial spectrum calculated using failed weights of this round will be distorted and the weights fluctuate significantly with respect to the previous round. The failure of multiple weights will result in the failure of the entire algorithm. Therefore, it is necessary to compare the difference between the weights of adjacent rounds with the divergence threshold THd after each round. When most of the weights in a round change more than THd, this round of iteration is considered a failure; then, the iteration is terminated and the result of the previous round is selected as the final result.

There is no need to decide whether to stop iteration for the first two iterations, because THd requires the difference between the weights of the first two rounds. The third and subsequent iterations need to determine whether to stop or not. That is because the first iteration of the response-shaping weights does not contain any information about the target locations, and the second iteration is the first one which does contain target information. Subsequent iterations just contain better target information.

Each iteration has M weights, corresponding to M angle regions. Compare the M weights of the previous iteration with the weights of the next iteration; if the difference between a set of corresponding weight vectors is less than TH, it is considered that the weight of this angle region converges. If it is greater than THd, the weight of this angle region is considered to diverge. When 10% of these M regions are considered convergent or divergent, the entire algorithm stops.

The entire algorithm process is shown in Algorithm 1.

Algorithm 1. IC-WORD algorithm

Input: original signal S_r, sidelobe level $A_{sidelobe}$
the convergence threshold TH
Output: spatial spectrum SP
(1) Calculated the weight of the first iteration $\mathbf{w}_{1st}$ according to the set sidelobe level $A_{sidelobe}$
(2) Calculate SP_{1st} by $\mathbf{w}_{1st}$ and S_r
(3) Design the weight of the next iteration $\mathbf{w}_{2nd}$ according to SP_{1st}
(4) Calculate SP_{2nd} by $\mathbf{w}_{2nd}$ and S_r
(5) Confirm the divergence threshold THd
(6) Calculate the next generation of $\mathbf{w}_{Nth}$ and SP_{Nth}
(7) If the difference between generations is less than TH enter (8);
Else if more than THd, enter (9);
Otherwise return to (6);
(8) Output SP_{Nth}
(9) Output $\mathrm{SP}_{(N-1)th}$

4. Simulations and Verification

4.1. 1~4 Iterations of IC-WORD under Multi-Coherent Source Conditions

TDM-MIMO mode is set to T3R4. There is a total of three transmitting elements spaced twice the wavelength, and four receiving elements spaced half the wavelength; the array arrangement diagram is shown below.

Figure 13 shows the spatial position of the antennas, with blue circles representing the transmitting array and red triangles representing the receiving array. Transmitting array elements take turns to transmit LFM signal. The number of signal sampling points within a single cycle is 128, totaling 512 cycles; LFM signal's starting frequency is set to 10 Mhz, bandwidth 300 kHz, and Gaussian white noise is added with a signal-to-noise ratio of 10 dB. Moreover, six simulated targets are set in different directions at a distance of 80 km from the radar, with speeds of 0. The specific parameters are shown in Table 2.

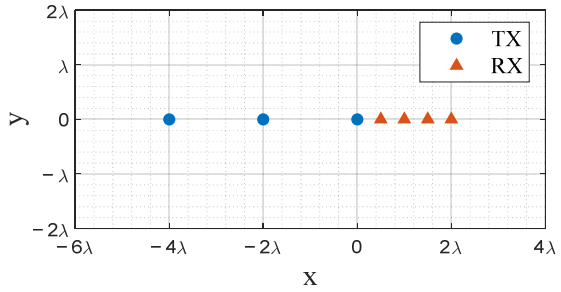

Figure 13. T3R4-MIMO array.

Table 2. Simulation parameters.

Radar Parameters	
MIMO	T3R4
Cycle number	512
Number of samples within a cycle	128
Starting frequency	10 MHz
Bandwidth	300 kHz
Target Parameters	
Quantity	6
Distance	Both are 80 km
Speed	0
Angle	$-60°$, $-20°$, $-10°$, $0°$, $30°$, $60°$
Signal-to-noise ratio	10 dB

The scanning range ($-90°$~$90°$) is divided into 180 regions at $1°$ intervals, and M is 180. The IC-WORD algorithm iterates four rounds in total and obtains four sets of weights: $\mathbf{w}_{1st}\mathbf{w}_{2nd}\mathbf{w}_{3rd}\mathbf{w}_{4th}$, where the spatial power spectrum calculated by the first three sets of weights ($\mathbf{w}_{1st}\mathbf{w}_{2nd}\mathbf{w}_{3rd}$) is shown in the following figure.

The comparison of the spatial spectrum estimation of 1~3 iterations is shown in Figure 14 and the details of them are displayed as the lower four panels (Figure 15). The green line is the spatial spectrum obtained from the first iteration of the IC-WORD algorithm (IC-WORD-1st), the red line is the spatial spectrum obtained from the second iteration (IC-WORD-2nd), and the blue line is the spatial spectrum obtained from the second iteration(IC-WORD-3rd). The dotted red lines represent the direction of the targets.

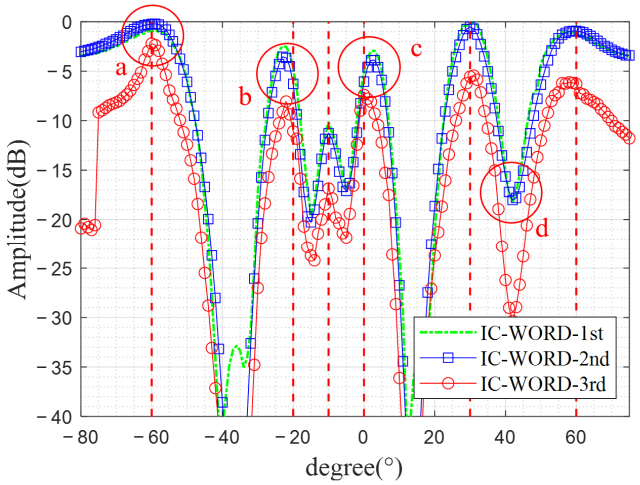

Figure 14. IC-WORD algorithm 1~3 iterations of spatial spectrum estimation.

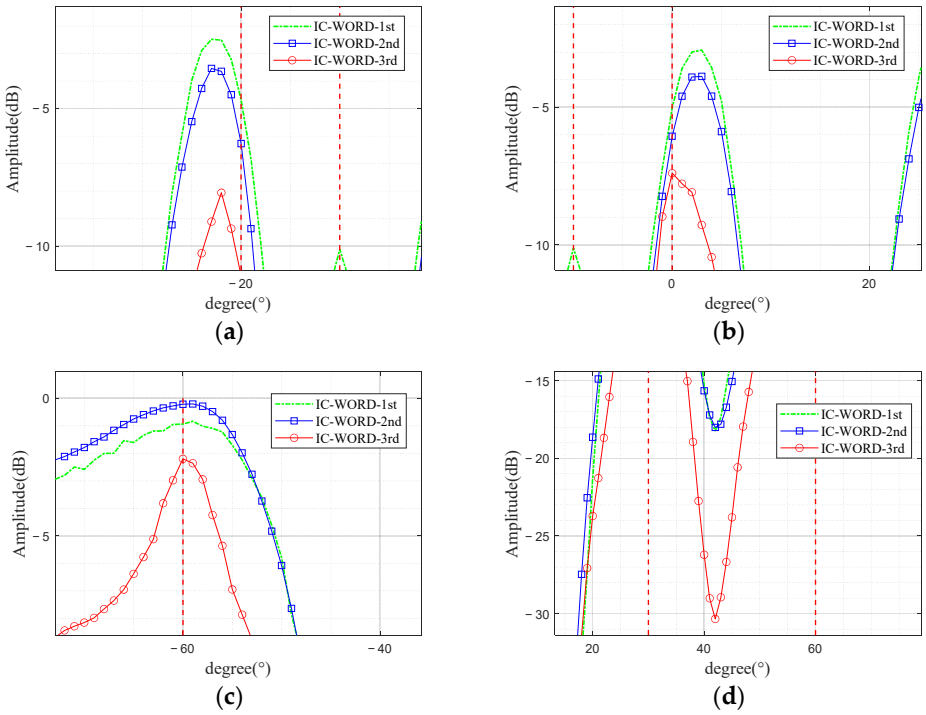

Figure 15. Details of the spatial spectrum: (**a**) −35°~−5°, (**b**) −5°~20°, (**c**) −70°~−40°, (**d**) 20°~80°.

In the process of spatial spectrum estimation, there is a common problem: when there are interferences or other targets in the vicinity of a single target, the spectral peak of that target will be affected by the spectral peaks of others, resulting in an unexpected shift, while the IC-WORD algorithm can largely mitigate this effect as the iteration progresses. The above comparison shows that, as the number of iterations increases, the spectral peaks of the targets that are affected and caused are shifted gradually correct back to their true directions (Figure 15a,b), and become sharper (Figure 15c); at the same time, the depressions between different targets deepen (Figure 15d), which means higher angular resolution and higher measurement accuracy are achieved.

The divergence problem of the algorithm is shown in the process of the fourth iteration, and the comparison of the spatial spectrum calculated in the third and fourth iterations is shown in the following figure.

As shown Figure 16, the spatial spectrum obtained from the fourth iteration shows extremely unstable jumps compared to the third, and the spectral peaks of targets appear

split and spiked. The appearance of this phenomenon indicates that some designs in the fourth set of weights $\mathbf{w}_{4th}$ failed, i.e., the criteria of the desired pattern were not met within a finite number of cycles. The angular regions corresponding to the failed weights are the regions where spikes appear, and the power calculated using the pattern distortion weights in these regions is abnormal, resulting in abrupt changes and splits in the spatial spectrum.

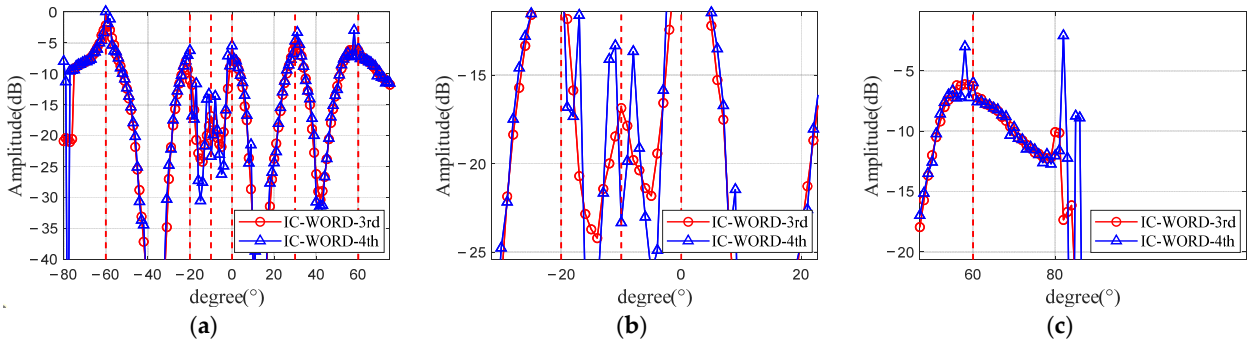

Figure 16. (**a**) IC-WORD algorithm 3rd and 4th iterations of spatial spectrum estimation. (**b**) Details of –25°~5°. (**c**) Details of 50°~80°.

If 10% of the weight design fails in one iteration, it is considered that the whole iteration is failed, which means the algorithm should be terminated, and the failure ratio of weights used to determine whether the algorithm needs to be terminated can be adjusted according to the actual situation.

Using the weights $\mathbf{w}_{61_1}\mathbf{w}_{61_2}\mathbf{w}_{61_3}\mathbf{w}_{61_4}$ corresponding to the $-30°$ angle region in the four sets as an example, their array patterns are shown below.

Array patterns corresponding to the weights of the $-30°$ regions (61st of the set for each of the four iterations) generated in the four iterations are compared in Figure 17 (Figure 17a: $\mathbf{w}_{61_1}$, Figure 17b: $\mathbf{w}_{61_2}$, Figure 17c: $\mathbf{w}_{61_3}$, Figure 17d: $\mathbf{w}_{61_4}$), where P_0, P_{dm} is the initial and desired pattern, and P_m is the result under this requirement.

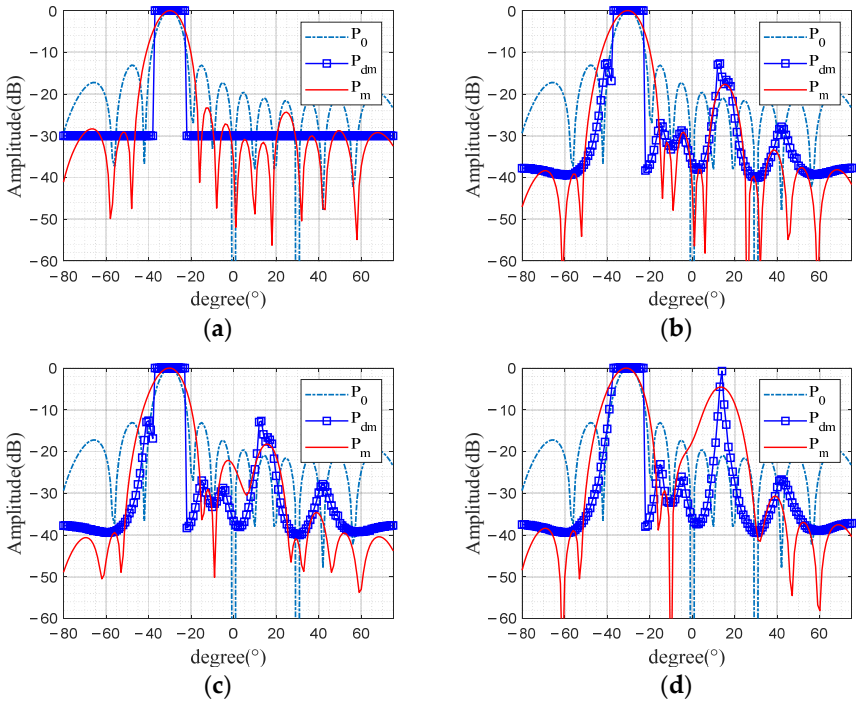

Figure 17. Array patterns corresponding to $\mathbf{w}_{61_1}\mathbf{w}_{61_2}\mathbf{w}_{61_3}\mathbf{w}_{61_4}$ generated by the IC-WORD algorithm: (**a**) $\mathbf{w}_{61_1}$, (**b**) $\mathbf{w}_{61_2}$, (**c**) $\mathbf{w}_{61_3}$, (**d**) $\mathbf{w}_{61_4}$.

The array pattern corresponding to the weight represents the response characteristics of the array to different directions after being weighted. With no information in the first iteration, there is no fluctuation in the sidelobe of $\mathbf{w}_{61_1}$'s pattern; $\mathbf{w}_{61_2}$'s pattern of the second iteration forms a certain width of zero trap in multiple directions, where SP_{1st} has peaks on the basis of the first iteration to ensure that the current angular power is calculated with minimal influence from the other directions to achieve higher angular accuracy and angular resolution; the third iteration is not much different from the second, and it can be found that the patterns of the first three iterations fit well with the desired ones, i.e., the weights are successfully designed. Compared to the previous, weight design of the fourth iteration is not so successful because the sidelobe of the desired pattern is so high and so sharp that the weights cannot reach and a distorted sidelobe with a width of about 20° and an amplitude of −4 dB is formed in the 15° direction, resulting in a large gap with P_{dm}. Finally, the fourth design fails and cannot be used to calculate the spatial spectrum.

To show the comparison of the weight adjustment process with the divergence threshold THd and convergence threshold TH, scatter plots of the weights in the complex coordinate system are drawn, and the results are shown in the following figure.

Figure 18a shows the comparison of the first three weights $\mathbf{w}_{61_1}\mathbf{w}_{61_2}\mathbf{w}_{61_3}$, where the blue scatter is $\mathbf{w}_{61_1}$, the red is $\mathbf{w}_{61_2}$, and the yellow is $\mathbf{w}_{61_3}$, and single weight values generated in different iterations of the same channel are connected by a line. It can be observed that the difference between $\mathbf{w}_{61_1}$ of blue scatter and $\mathbf{w}_{61_2}$ of red scatter is much larger than the difference between $\mathbf{w}_{61_2}$ and $\mathbf{w}_{61_3}$. The convergence threshold TH is set to 5×10^{-2}, and the difference between $\mathbf{w}_{61_2}$ and $\mathbf{w}_{61_3}$ has already met the algorithm termination condition.

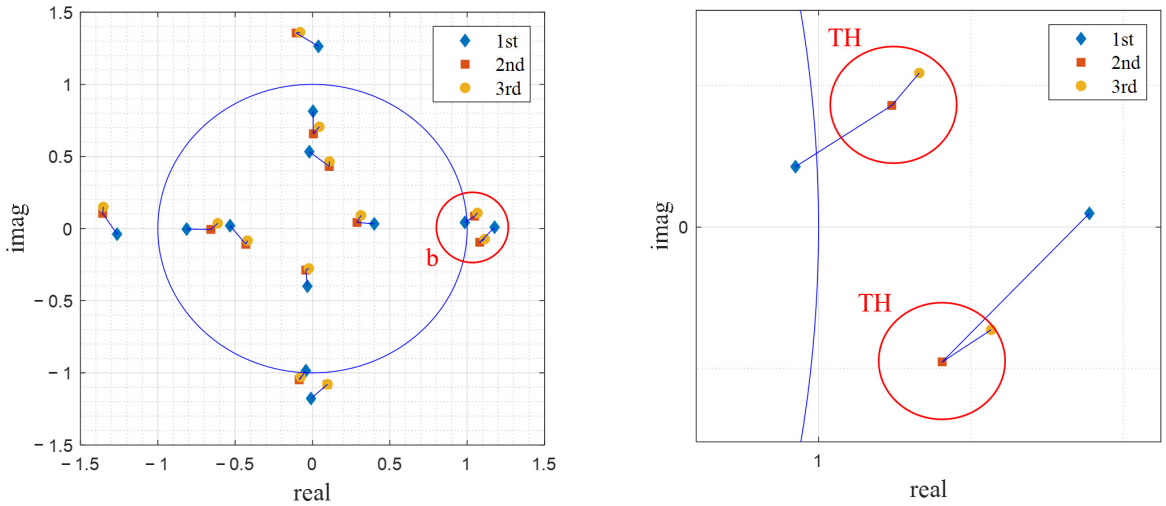

Figure 18. Scatter plots of $\mathbf{w}_{61_1}\mathbf{w}_{61_2}\mathbf{w}_{61_3}$: (**a**) whole, (**b**) detail.

Adding the fourth weight to the figure, $\mathbf{w}_{61_1}\mathbf{w}_{61_2}\mathbf{w}_{61_3}\mathbf{w}_{61_4}$ of four iterations are compared as shown in the following figure.

As shown in Figure 19, the first three weights are still blue, red, and yellow, with added purple points of weights $\mathbf{w}_{61_4}$ from the fourth iterations. It can be observed that the purple scatter of the fourth weights $\mathbf{w}_{61_4}$ deviates severely from the third weights $\mathbf{w}_{61_3}$, and the difference is greater than the difference between $\mathbf{w}_{61_1}$ and $\mathbf{w}_{61_2}$, namely the divergence threshold THd, which can be considered a failed design. In the fourth round, there are multiple failed weights such as $\mathbf{w}_{61_4}$, so the fourth iteration is considered invalid.

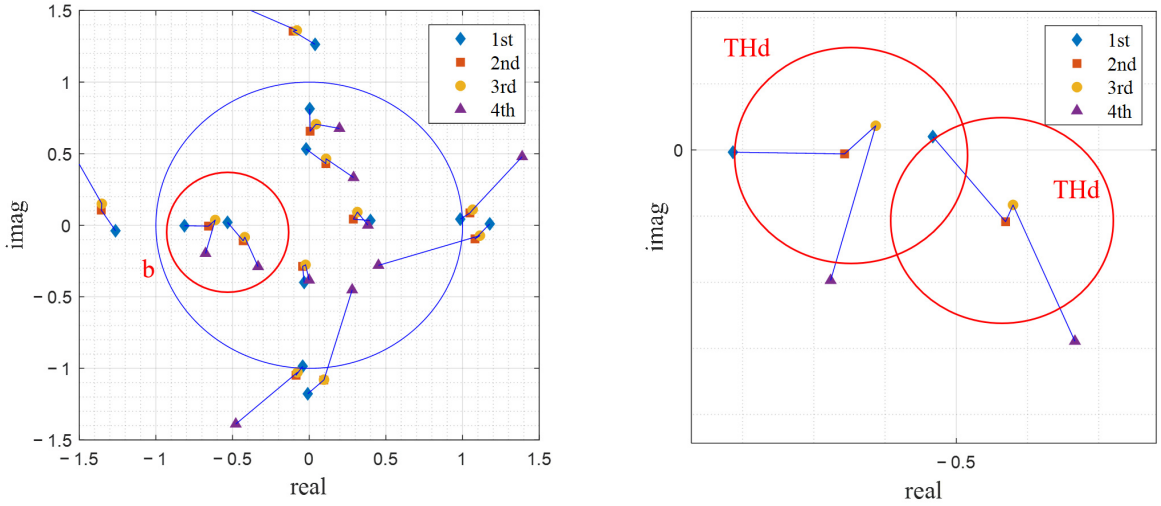

Figure 19. Scatter plots of $\mathbf{w}_{61_1}\mathbf{w}_{61_2}\mathbf{w}_{61_3}\mathbf{w}_{61_4}$: (**a**) whole, (**b**) detail.

4.2. Comparison of the Spatial Spectrum Estimation between Smooth-MUSIC and IC-WORD under Multi-Coherent Source Conditions

Simulation parameters still follow the parameters set in Section 4.1. Firstly, the target located at $-10°$ is removed, and the algorithm comparison between Smooth-MUSIC and IC-WORD is carried out under the five-target condition, as shown in the left figure below.

In Figure 20, the green line is the spatial spectrum obtained from the first iteration of the IC-WORD algorithm (IC-WORD-1st), the red line is the spatial spectrum obtained from the second iteration (IC-WORD-2nd), and the blue line is calculated by the Smooth-MUSIC algorithm. The dotted red lines represent the direction of the targets.It's obvious that both algorithms can detect five peaks in the spatial spectrum under the five-targets condition.

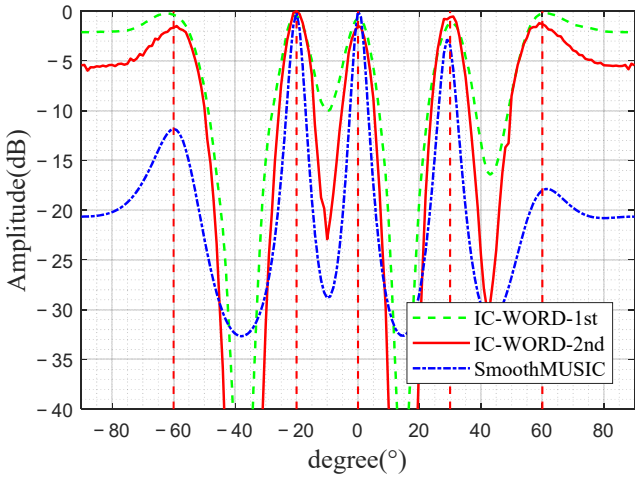

Figure 20. Comparison between smooth-MUSIC method and IC-WORD method under the five-targets ($-60°$, $-20°$, $0°$, $30°$, and $60°$) condition.

To show the difference, the target located at $-10°$ is added back to the simulation and the comparison of the two algorithms observed under the conditions of six targets. The simulation results are shown in Figure 21.

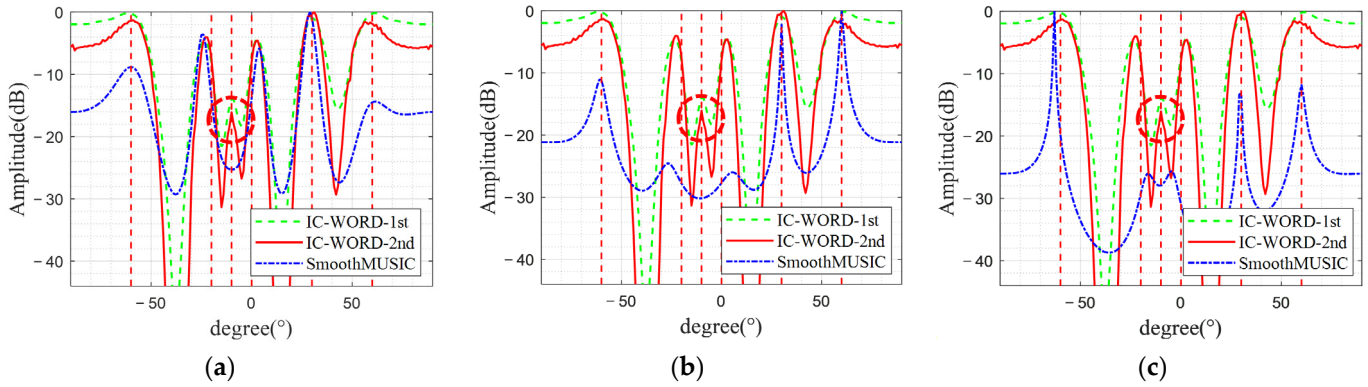

Figure 21. Comparison of Smooth-MUSIC and IC-WORD under the six targets (−60°, −20°, −10°, 0°, 30°, and 60°) condition. (Subarray array element number: (**a**) 4, (**b**) 6, (**c**) 7).

In Figure 21, the green line is the spatial spectrum obtained from the first iteration of the IC-WORD algorithm (IC-WORD-1st), the red line is the spatial spectrum obtained from the second iteration (IC-WORD-2nd), and the blue line is calculated by the Smooth-MUSIC algorithm. The dotted red lines represent the direction of the targets. Since the mode of TDM-MIMO is set to T3R4, the virtual aperture of the array is 12 elements, and Smooth-MUSIC obtains, at most, five peaks under this condition. Figure 14 show the comparison between the proposed IC-WORD algorithm and Smooth-MUSIC algorithm under the conditions of six coherent targets, respectively. When there are five targets in the same distance unit, both the IC-WORD algorithm and Smooth-MUSIC algorithm can successfully detect five peaks; however, when the number of targets increases to six, No matter how the number of elements in the sub-array is adjusted, the Smooth-MUSIC algorithm fails but IC-WORD can still detect six targets (the red dotted circle in Figure 21 shows the difference), which proves that IC-WORD breaks the limit of the maximum detectable targets of the general spatial smoothing algorithm. Moreover, compared to Smooth-MUSIC, the spectral peaks' direction of IC-WORD is closer to the true target angle, indicating that the algorithm has higher DOA estimation accuracy.

4.3. Verification of Measured Data

The measured data come from a high-frequency surface wave radar station in southern China, which was obtained in May 2022. The Range–Doppler (RD) spectrum is shown below.

As shown in the Figure 22, since the distance and speed between multiple coherent targets in these data are basically the same, they overlap to a point in RD spectrum and can only be resolved by angle dimension, i.e., distinguished through range–angle (RA) spectrum or angle–Doppler (AD) spectrum. The following Figure 23 is a comparison of the processing results of measured data between traditional methods and the IC-WORD algorithm.

The RA spectrum and AD spectrum is shown in the figure above. Compared with the conventional algorithm, the measured data of HFSWR are used to verify the advantages of IC-WORD algorithm, which has lower sidelobe and narrower main lobe. This article focuses on the three targets with the same distance and speed in the data, among which the two targets at 0° and 20° have stronger echoes and the other one around −30° has weaker echo. The data processing mode of the three images on the top is the conventional method, while, on the bottom, is IC-WORD. The three images from left to right are, respectively, the AD spectrum, RA spectrum, and the target schematic diagram after the threshold judgment. It can be observed that, in the same threshold range, the conventional method in RA spectrum is capable of detecting two targets located at about 0° and 20°. However, due to low angular resolution, the peaks of Target1 and Target2 are mixed and the sidelobe of strong targets (Target1, 2) overwhelm the weak target (Target3). Meanwhile, the angle resolution of IC-WORD is higher, so the two peaks are completely separated and the

sidelobe of IC-WORD is lower, so the target at -30° is successfully extracted from the sidelobe of strong targets. Finally, the three targets were all detected successfully.

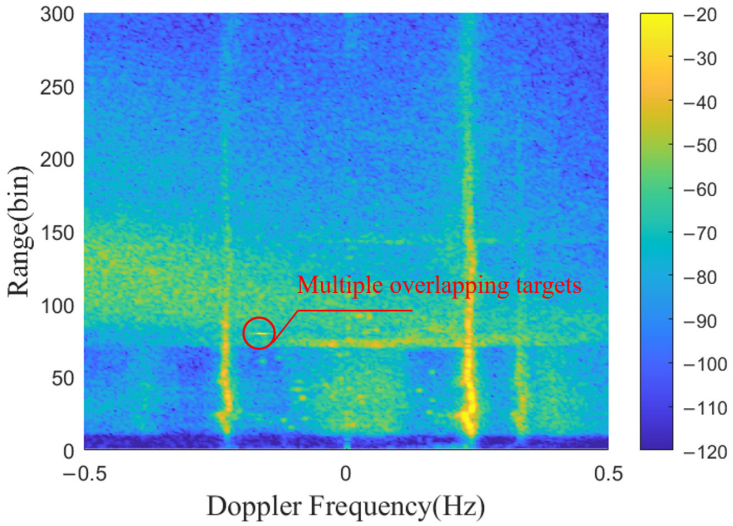

Figure 22. RD spectrum obtained by processing the measured data obtained in May 2022.

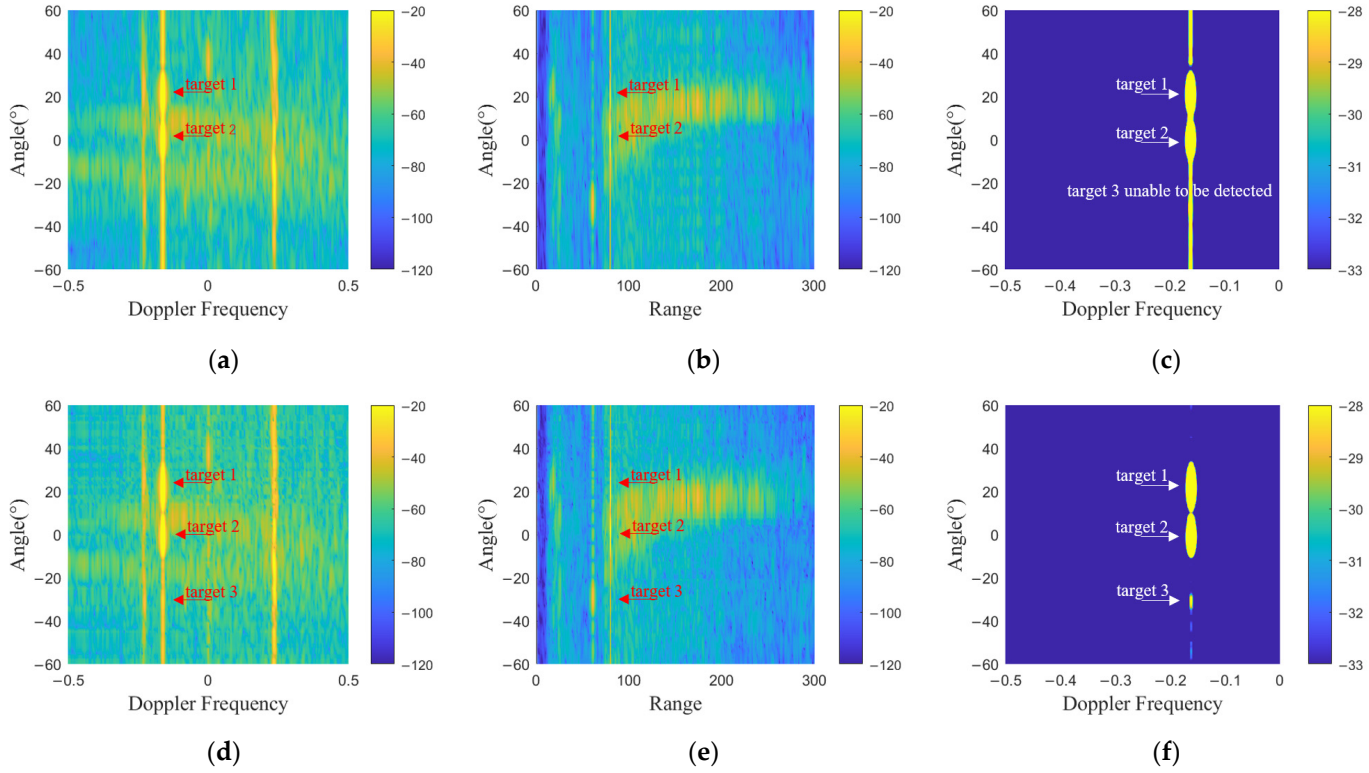

Figure 23. AD/RA spectrum of the measured data; (**a**) AD spectrum processed by traditional method; (**b**) RA spectrum processed by traditional method; (**c**) RA spectrum after threshold judgment; (**d**) AD spectrum processed by IC-WORD; (**e**) RA spectrum processed by IC-WORD; (**f**) RA spectrum processed by IC-WORD after threshold judgment.

4.4. Algorithm Performance Comparison

The radar parameters are the same as those set in Section 4.1 and the target is set as five targets (-60°, -20°, 0°, 30°, and 60°). At this time, both algorithms are effective. The signal-to-noise ratio (SNR) is gradually improved, the average value of the difference between the peaks' angles of five targets and the actual target angles is calculated, and

repeated experiments are conducted to calculate the DOA estimation's root mean squared error (RMSE). The results are shown in the Figure 24:

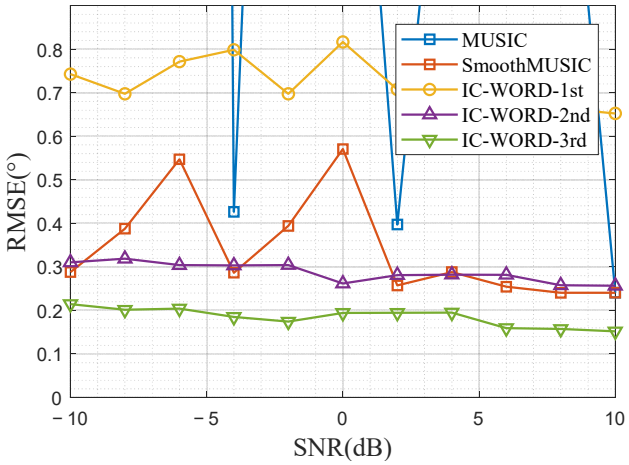

Figure 24. Comparison of angular RMSE changes with SNR between Smooth-MUSIC and IC-WORD.

As shown above, the blue line is the RMSE in DOA estimation of the MUISC algorithm that fails under the coherence condition, the red is the RMSE of Smooth-MUSIC used for decoherence, and the yellow/purple/green are the accuracy of the first three iterations of the IC-WORD algorithm, respectively, and it can be observed that IC-WORD is better than the Smooth-MUSIC algorithm after the second iteration with the same SNR.

By controlling the number of transmitting and receiving array elements the maximum number of detectable coherent targets can be compared between two algorithms in different MIMO modes.

Detailed process: place targets at the same interval within the detectable range $[-90°, 90°]$ to ensure maximum distinguishability. Gradually increase the number of targets until there are targets that cannot be distinguished from the spatial spectrum results. Based on the results, determine the maximum detectable targets.

As for the problem of changing the MIMO mode, the process of the experiment is to select several channels of a large MIMO array for processing and change the number of channels selected which can change the corresponding MIMO mode of the experiment.

The results are in Figure 25.

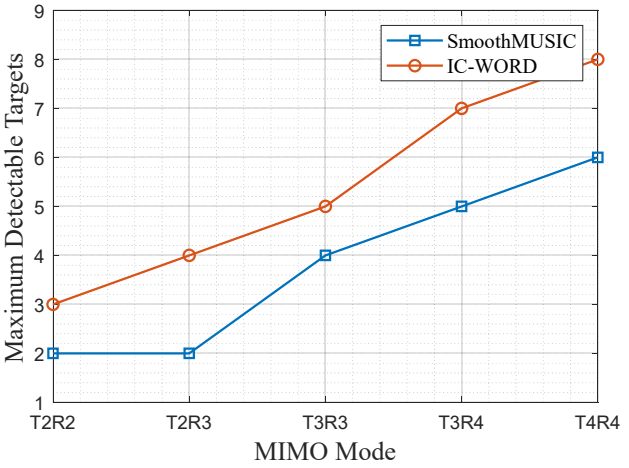

Figure 25. Comparison of maximum detectable coherent targets between Smooth-MUSIC and IC-WORD.

The proposed IC-WORD algorithm outperforms the Smooth-MUSIC algorithm in the above MIMO modes in terms of the maximum number of detectable coherent targets.

In summary, the IC-WORD algorithm proposed in this paper has obvious advantages and improvements over the conventional spatial smoothing algorithm in DOA estimation of multi-coherent sources in the high-frequency TDM-MIMO radar regime.

5. Conclusions

The main contribution of this work is a DOA estimation method of multi-coherent target based on weight vector orthogonal decomposition (IC-WORD) for MIMO-HFSWR. Firstly, the accurate control of the pattern is realized based on the weight vector orthogonal decomposition algorithm (WORD). Secondly, on the basis of WORD, the IC-WORD algorithm is proposed to accurately estimate the direction of multiple coherent targets. By analyzing the echo, sidelobes are designed to have specific shapes as the iteration goes on, which minimize the impact of coherent signals or interference in other directions when estimating the target in the current direction, and the angle can be obtained very accurately.

This work not only carries out simulation analysis, but also uses measured data to verify the feasibility of IC-WORD. The results all indicate that, when there are multiple coherent targets that overlap to a point in RD spectrum, the IC-WORD algorithm has the following advantages:

1. Eliminating the peak shift caused by nearby targets or interference by iteration.
2. Gradually achieving high DOA estimation accuracy through iteration.
3. Still valid when the traditional spatial smoothing algorithm fails due to an excessive number of coherent objects.

As for future direction, it would be worthwhile to add control over the main lobe of the pattern and attempt to suppress main-lobe interference.

Author Contributions: Conceptualization, Q.Y. and Y.L.; methodology, Y.L.; software, Y.L.; validation, Q.Y. and Y.L.; formal analysis, X.Z.; investigation, X.Z.; resources, Q.Y.; data curation, Y.L.; writing—original draft preparation, Y.L.; writing—review and editing, Q.Y.; project administration, Y.L.; funding acquisition, Q.Y. All authors have read and agreed to the published version of the manuscript.

Funding: This work was supported in part by the National Natural Science Foundation of China under Grant 62031014 and Technology Foundation Project of the Ministry of Industry and Information Technology under Grant JSQB2020603A001.

Data Availability Statement: Restrictions apply to the availability of the data, which were used under license for this study. Data are available from the authors with permission from the Key Laboratory of Marine Environmental Monitoring and Information Processing.

Acknowledgments: The authors truly thank the Key Laboratory of Marine Environmental Monitoring and Information Processing, Harbin Institute of Technology, China, for data support.

Conflicts of Interest: The authors declare no potential conflict of interest.

References

1. Dzvonkovskaya, A.; Helzel, T.; Petersen, L.; Merz, C.R.; Liu, Y.; Weisberg, R.H. Initial results of ship detection and tracking using WERA HF ocean radar with MIMO configuration. In Proceedings of the 2014 15th International Radar Symposium (IRS), Gdańsk, Poland, 16–18 June 2014; pp. 1–3.
2. Dzvonkovskaya, A.; Merz, C.R.; Liu, Y.; Weisberg, R.H.; Helzel, T.; Petersen, L. Initial surface current measurements on the West Florida shelf using WERA HF ocean radar with multiple input multiple output (MIMO) synthetic aperture. In Proceedings of the 2014 Oceans, St. John's, NL, Canada, 14–19 September 2014; pp. 1–4.
3. Jangal, F.; Menelle, M. French HFSWR contribution to the European integrated maritime surveillance system I2C. In Proceedings of the IET International Radar Conference 2015, Hangzhou, China, 14–16 October 2015; pp. 1–5.
4. Tan, J.; Wen, B.; Tian, Y.; Tian, M. Use of a time-staggered FMCW signal for portable high-frequency surface wave radar. *Remote Sens. Lett.* **2016**, *7*, 1180–1189. [CrossRef]
5. Viberg, M.; Krim, H. Two decades of statistical array processing. In Proceedings of the Conference Record of the Thirty-First Asilomar Conference on Signals, Systems and Computers (Cat. No.97CB36136), Pacific Grove, CA, USA, 2–5 November 1997; Volume 771, pp. 775–777.

6. Capon, J. High-resolution frequency-wavenumber spectrum analysis. *Proc. IEEE* **1969**, *57*, 1408–1418. [CrossRef]
7. Paulraj, A.; Roy, R.; Kailath, T. A subspace rotation approach to signal parameter estimation. *Proc. IEEE* **1986**, *74*, 1044–1046. [CrossRef]
8. Viberg, M.; Ottersten, B. Sensor array processing based on subspace fitting. *IEEE Trans. Signal Process.* **1991**, *39*, 1110–1121. [CrossRef]
9. Viberg, M.; Ottersten, B.; Kailath, T. Detection and estimation in sensor arrays using weighted subspace fitting. *IEEE Trans. Signal Process.* **1991**, *39*, 2436–2449. [CrossRef]
10. Hung, H.; Kaveh, M. Coherent wide-band ESPRIT method for directions-of-arrival estimation of multiple wide-band sources. *IEEE Trans. Acoust. Speech Signal Process.* **1990**, *38*, 354–356. [CrossRef]
11. Jiang, X.; Qian, S. DOA estimation of coherent signals based on modified music algorithm. In Proceedings of the 2021 IEEE 3rd International Conference on Civil Aviation Safety and Information Technology (ICCASIT), Changsha, China, 20–22 October 2021; pp. 918–921.
12. Rahamim, D.; Tabrikian, J.; Shavit, R. Source localization using vector sensor array in a multipath environment. *IEEE Trans. Signal Process.* **2004**, *52*, 3096–3103. [CrossRef]
13. Iwai, T.; Hirose, N.; Kikuma, N.; Sakakibara, K.; Hirayama, H. DOA estimation by MUSIC algorithm using forward-backward spatial smoothing with overlapped and augmented arrays. In Proceedings of the 2014 International Symposium on Antennas and Propagation Conference Proceedings, Kaohsiung, Taiwan, 2–5 December 2014; pp. 375–376.
14. Liyang, Z.; Dengshan, H. A new ESPRIT algorithm based on Toeplitz method for coherent signals. In Proceedings of the 2011 International Conference on Transportation, Mechanical, and Electrical Engineering (TMEE), Changchun, China, 16–18 December 2011; pp. 1521–1524.
15. Li, D.; Dong, C.; Huang, J. A study on the application of Toeplitz approximation method on DOA estimation. In Proceedings of the 2010 2nd International Conference on Signal Processing Systems, Dalian, China, 5–7 July 2010; pp. V3-215–V3-218.
16. Vasylyshyn, V. Selecting the Best DOA Estimates among Estimates Obtained using Toeplitz Matrix Approximation and General Covariance Matrix. In Proceedings of the 2020 17th European Radar Conference (EuRAD), Utrecht, The Netherlands, 10–15 January 2021; pp. 294–297.
17. Vasylyshyn, V. Threshold Performance Improvement of DOA Estimation using Pseudo-Noise Resampling and Toeplitz Covariance Matrix Approximation. In Proceedings of the 2020 IEEE Ukrainian Microwave Week (UkrMW), Kharkiv, Ukraine, 21–25 September 2020; pp. 40–43.
18. Zhao, Y.; Zhou, Y.; Yang, Y.; Hao, Y. Robust Virtual Array Transformation Beamforming Approach Against Jammer Motion. In Proceedings of the 2019 International Applied Computational Electromagnetics Society Symposium—China (ACES), Nanjing, China, 8–11 August 2019; pp. 1–2.
19. Stoica, P.; Moses, R.L.; Friedlander, B.; Soderstrom, T. Maximum likelihood estimation of the parameters of multiple sinusoids from noisy measurements. *IEEE Trans. Acoust. Speech Signal Process.* **1989**, *37*, 378–392. [CrossRef]
20. Stoica, P.; Nehorai, A. MUSIC, maximum likelihood and Cramer-Rao bound: Further results and comparisons. In Proceedings of the International Conference on Acoustics, Speech, and Signal Processing, Glasgow, UK, 23–26 May 1989; Volume 2604, pp. 2605–2608. [CrossRef]
21. Stoica, P.; Nehorai, A. MUSIC, maximum likelihood, and Cramer-Rao bound: Further results and comparisons. *IEEE Trans. Acoust. Speech Signal Process.* **1990**, *38*, 2140–2150. [CrossRef]
22. Wagner, M.; Gerstoft, P.; Park, Y. Gridless DOA Estimation via. Alternating Projections. In Proceedings of the ICASSP 2019—2019 IEEE International Conference on Acoustics, Speech and Signal Processing (ICASSP), Brighton, UK, 12–17 May 2019; pp. 4215–4219.
23. Lei, H.; Shunjun, W.; Linrang, Z. Low-complexity method of weighted subspace fitting for direction estimation. In Proceedings of the IEEE International Radar Conference, Arlington, VA, USA, 9–12 May 2005; pp. 491–496.
24. Lee, D. MIMO OFDM Channel Estimation via Block Stagewise Orthogonal Matching Pursuit. *IEEE Commun. Lett.* **2016**, *20*, 2115–2118. [CrossRef]
25. Tan, Z.; Nehorai, A. Sparse Direction of Arrival Estimation Using Co-Prime Arrays with Off-Grid Targets. *IEEE Signal Process. Lett.* **2014**, *21*, 26–29. [CrossRef]
26. Hua, X.; Ono, Y.; Peng, L.; Cheng, Y.; Wang, H. Target Detection Within Nonhomogeneous Clutter Via Total Bregman Divergence-Based Matrix Information Geometry Detectors. *IEEE Trans. Signal Process.* **2021**, *69*, 4326–4340. [CrossRef]
27. Hua, X.; Ono, Y.; Peng, L.; Xu, Y. Unsupervised Learning Discriminative MIG Detectors in Nonhomogeneous Clutter. *IEEE Trans. Commun.* **2022**, *70*, 4107–4120. [CrossRef]
28. Zhang, X.; He, Z.; Liao, B.; Zhang, X.; Peng, W. Pattern Synthesis for Arbitrary Arrays via Weight Vector Orthogonal Decomposition. *IEEE Trans. Signal Process.* **2018**, *66*, 1286–1299. [CrossRef]
29. Zhang, X.; He, Z.; Xia, X.G.; Liao, B.; Zhang, X.; Yang, Y. OPARC: Optimal and Precise Array Response Control Algorithm—Part II: Multi-Points and Applications. *IEEE Trans. Signal Process.* **2019**, *67*, 668–683. [CrossRef]